ISSN 1674-1056
http://cpb.iphy.ac.cn
http://iopscience.iop.org/cpb
中国物理 B
Chinese Physics
中国物理 Chinese Physics B

Collapses-revivals phenomena induced by weak magnetic flux in diamond chain

Na-Na Chang(常娜娜)[1], Wen-Quan Jing(景文泉)[2], Yu Zhang(张钰)[1], Ai-Xia Zhang(张爱霞)[2], Ju-Kui Xue(薛具奎)[2], Su-Peng Kou(寇谡鹏)[1]

Citation: Chin. Phys. B . 2020, 29(1): 010306 . **doi:** 10.1088/1674-1056/ab6087
Journal homepage: http://cpb.iphy.ac.cn; http://iopscience.iop.org/cpb

What follows is a list of articles you may be interested in

Atom-pair tunneling and quantum phase transition in asymmetry double-well trap in strong-interaction regime

Ji-Li Liu(刘吉利)[1], Jiu-Qing Liang(梁九卿)[2]

Chin. Phys. B . 2019, 28(11): 110304 . **doi:** 10.1088/1674-1056/ab44b6

Manipulating transition of a two-component Bose-Einstein condensate with a weak *δ*-shaped laser

Bo Li(李博), Xiao-Jun Jiang(蒋小军), Xiao-Lin Li(李晓林), Wen-Hua Hai(海文华), Yu-Zhu Wang(王育竹)

Chin. Phys. B . 2019, 28(10): 100303 . **doi:** 10.1088/1674-1056/ab3e64

Simulation and measurement of millimeter-wave radiation from Josephson junction array

Xin Zhang(张鑫), Sheng-Hui Zhao(赵生辉), Li-Tian Wang(王荔田), Jian Xing(邢建), Sheng-Fang Zhang(张胜芳), Xue-Lian Liang(梁雪连), Ze He(何泽), Pei Wang(王培), Xin-Jie Zhao(赵新杰), Ming He(何明), Lu Ji(季鲁)

Chin. Phys. B . 2019, 28(6): 060305 . **doi:** 10.1088/1674-1056/28/6/060305

Ground-state vortex structures of a rotating binary dipolar Bose-Einstein condensate confined in harmonic plus quartic potential

Guang-Ping Chen(陈光平), Chang-Bing Qiao(乔昌兵), Hui Guo(郭慧), Lin-Xue Wang(王林雪), Ya-Jun Wang(王雅君), Ren-Bing Tan(谭仁兵)

Chin. Phys. B . 2019, 28(1): 010308 . **doi:** 10.1088/1674-1056/28/1/010308

Current-phase relations of a ring-trapped Bose-Einstein condensate with a weak link

Xiu-Rong Zhang(张秀荣), Wei-Dong Li(李卫东)

Chin. Phys. B . 2019, 28(1): 010303 . **doi:** 10.1088/1674-1056/28/1/010303

Collapses-revivals phenomena induced by weak magnetic flux in diamond chain*

Na-Na Chang(常娜娜)[1,†], Wen-Quan Jing(景文泉)[2], Yu Zhang(张钰)[1], Ai-Xia Zhang(张爱霞)[2], Ju-Kui Xue(薛具奎)[2], and Su-Peng Kou(寇谡鹏)[1,‡]

[1] *Department of Physics, Beijing Normal University, Beijing* 100875, *China*
[2] *College of Physics and Electronics Engineering, Northwest Normal University, Lanzhou* 730070, *China*

(Received 19 August 2019; revised manuscript received 13 November 2019; accepted manuscript online 11 December 2019)

We investigate the quantum dynamical behaviors of bosons in a diamond chain with weak magnetic flux (WMF), including Landau–Zener tunnelling, Bloch oscillations, localization phenomenon, and collapses-revivals phenomena. We observed that collapses-revivals phenomena can occur in diamond chain with WMF and cannot exist in the strong magnetic flux case as the previous study (Chang N N and Xue J K, 2018, *Chin. Phys. B* **27** 105203). Induced by WMF, the energy band for the system varies from gapless to gapped structure. The position of the extrema of probability amplitude for ground state can also be altered by WMF within a single diamond plaquette. As a consequence, the transitions between different dynamical behaviors of bosons in diamond chain can be manipulated by WMF, depending on its initial configurations.

Keywords: collapses-revivals phenomena, Bloch oscillations, Landau–Zener tunneling, localization phenomenon, flat band

PACS: 03.75.Lm, 05.30.Jp, 03.75.Mn, 67.85.Hj **DOI:** 10.1088/1674-1056/ab6087

1. Introduction

The experimental realization of cold atoms successfully accelerates certain typical quantum phenomena occurring in various optical lattices,[1–4] including Landau–Zener tunnelling, Bloch oscillations, localization phenomenon, and collapses-revivals phenomena, which are strongly associated with the energy structure of the system. Degenerate energy levels can be split and the gap between different energy bands can be opened by a perturbation embeded in a diamond chain,[5–9] such as synthetic gauge field, which provides a new potential for ultracold atom to simulate intriguing quantum phenomena in traditional condensed matter physics.[10–13] Optical lattice is a key platform to investigate the quantum behaviors by twisted bilayer graphene model,[14] Haldane model,[15] Kane–Mele model,[16] and Hofstadter butterfly model.[17–19]

As is known, particles exhibit Bloch oscillations in an optical lattice (periodic potential field). However, with the gapped energy levels, the Landau–Zener effect illustrates the tunnelling of particles among distinct bands for the system, which is based on the energy bias of three levels in diamond chain.[20–25] Flat band is a special case of the energy band structure for the system, which can be characterized by the compact localized states (CLSs),[6,26–29] *i.e.*, the eigenstates for the system, whose dynamical behavior exhibits nonzero amplitudes on certain lattice sites with a finite number.[5,6,27,28] This occurs due to destructive interference of geometric phases and has been observed recently in double-well potential,[30] Lieb photonic lattices,[31,32] kagome lattice,[29,33] diamond chain,[6,26,34] and sawtooth lattices.[35]

We consider a diamond chain subjected to a WMF, in which the transitions among various quantum phenomena are investigated by the characteristics of the ground states of the system. Induced by the WMF, the gap between different energy bands of the system varies from zero (gapless) to nonzero (gapped). Note that there exists a flat band. Furthermore, the position of the extrema of complex amplitude for the ground state can be affected by WMF. With various initial configurations of bosons, the tunnelling dynamics exhibits collapses-revivals phenomena, Landau–Zener tunnelling, Bloch oscillations, and localization phenomenon in diamond chain with WMF. Consequently, the transitions among various quantum phenomena both depend on WMF and the initial configurations of bosons in the diamond chain.

The paper is structured as follows. Section 2 introduces the tight-binding model in diamond chain and describes the computational method. The energy band structure and the characteristics of the ground state for the system are given in Section 3. Section 4 demonstrates the dynamiccal behaviors of bosons with various initial configurations. Finally, we give our conclusions in Section 5.

*Project supported the National Natural Science Foundation of China (Grant Nos. 11974053, 11674026, 11274255, 11305132, and 11475027) and China Scholarship Council (CSC).

†Corresponding author. E-mail: nnchangqq@gmail.com
‡Corresponding author. E-mail: spkou@bnu.edu.cn

© 2020 Chinese Physical Society and IOP Publishing Ltd

2. Tight-binding model

The Hamiltonian of bosons in a diamond chain (as shown in Fig. 1) is

$$\hat{H} = \sum_{n=1}^{N} \varepsilon n(\hat{a}_n^\dagger \hat{a}_n + \hat{b}_n^\dagger \hat{b}_n + \hat{c}_n^\dagger \hat{c}_n) + \frac{\varepsilon}{2}\hat{b}_n^\dagger \hat{b}_n - [(\hat{b}_n^\dagger \hat{a}_n + \hat{c}_n^\dagger \hat{b}_n)\,\mathrm{e}^{\mathrm{i}\phi} - \hat{b}_{n-1}^\dagger \hat{c}_n - \hat{a}_n^\dagger \hat{b}_{n-1} + \text{c.c.}], \quad (1)$$

where $\hat{a}_n^\dagger$, $\hat{b}_n^\dagger$, $\hat{c}_n^\dagger$ are the creation operators while $\hat{a}_n$, $\hat{b}_n$, and $\hat{c}_n$ are the annihilation operators, respectively. The particle number operator on a unit cell, $\hat{M}_n = \hat{a}_n^\dagger \hat{a}_n + \hat{b}_n^\dagger \hat{b}_n + \hat{c}_n^\dagger \hat{c}_n$ satisfies the normalization condition $\sum_{n=1}^{N}(|a_n|^2 + |b_n|^2 + |c_n|^2) = 1$.

The evolutional equations of a_n, b_n, and c_n are,

$$\begin{aligned}
\mathrm{i}\frac{\mathrm{d}a_n}{\mathrm{d}t} &= \varepsilon n a_n - \mathrm{e}^{-\mathrm{i}\phi} b_n - b_{n-1}, \\
\mathrm{i}\frac{\mathrm{d}b_n}{\mathrm{d}t} &= \varepsilon(n+\frac{1}{2})b_n - \mathrm{e}^{\mathrm{i}\phi} a_n - \mathrm{e}^{-\mathrm{i}\phi} c_n - c_{n+1} - a_{n+1}, \\
\mathrm{i}\frac{\mathrm{d}c_n}{\mathrm{d}t} &= \varepsilon n c_n - \mathrm{e}^{\mathrm{i}\phi} b_n - b_{n-1}, \qquad (2)
\end{aligned}$$

obtained from the Heisenberg equations of motion, $\mathrm{i}\,\mathrm{d}\hat{a}_n/\mathrm{d}t = [\hat{a}_n, H]$, $\mathrm{i}\,\mathrm{d}\hat{b}_n/\mathrm{d}t = [\hat{b}_n, H]$, and $\mathrm{i}\,\mathrm{d}\hat{c}_n/\mathrm{d}t = [\hat{c}_n, H]$, where we have taken $\hbar = 1$.

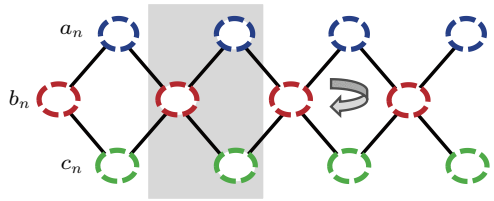


Fig. 1. The sketch of the diamond chain considered in Eq. (1) includes a, b, and c chains, which are characterized by the blue, red, and green dotted circles, respectively. There holds the horizontal tilting ε and the artificial magnetic field B with the magnetic flux ϕ in a single plaquette (gray arrow), which is perpendicular to diamond chain plane. Note that gray rectangle defines the n-th unit cell.

3. Properties of the system

When $\varepsilon = 0$, the eigenmodes of Eq. (1) are obtained using Fourier transform,

$$\begin{aligned}
a_n &= \frac{1}{2\pi}\int_{-\pi}^{\pi} a_k \mathrm{e}^{\mathrm{i}kn}\mathrm{d}k, \\
b_n &= \frac{1}{2\pi}\int_{-\pi}^{\pi} b_k \mathrm{e}^{\mathrm{i}kn}\mathrm{d}k, \\
c_n &= \frac{1}{2\pi}\int_{-\pi}^{\pi} c_k \mathrm{e}^{\mathrm{i}kn}\mathrm{d}k,
\end{aligned}$$

i.e.,

$$\mathrm{i}\dot{a}_k = H_k a_k, \quad \mathrm{i}\dot{b}_k = H_k b_k, \quad \mathrm{i}\dot{c}_k = H_k c_k, \qquad (3)$$

where

$$H_k = \begin{pmatrix} 0 & -(\mathrm{e}^{-\mathrm{i}\phi} + \mathrm{e}^{-\mathrm{i}k}) & 0 \\ -(\mathrm{e}^{\mathrm{i}\phi} + \mathrm{e}^{\mathrm{i}k}) & 0 & -(\mathrm{e}^{-\mathrm{i}\phi} + \mathrm{e}^{\mathrm{i}k}) \\ 0 & -(\mathrm{e}^{\mathrm{i}\phi} + \mathrm{e}^{-\mathrm{i}k}) & 0 \end{pmatrix}. \quad (4)$$

3.1. Spectrum

We obtain the energy spectrum $\lambda(k)$

$$\lambda(k)^3 + 4(1+\cos\phi\cos k)\lambda(k) = 0, \qquad (5)$$

resulting in three bands

$$\lambda_{\text{flat}} \equiv 0, \qquad (6)$$

$$\lambda_{\pm} = \pm 2\sqrt{-1-\cos\phi\cos k}, \qquad (7)$$

as shown in Fig. 2. The two dispersive energy bands touch the flat band at the edge of the Brillouin zone ($k = \pm\pi$), where we see a conical dispersion. The flat band is denoted by the yellow plane. Due to spatial inversion symmetry, the two dispersive energy bands are symmetric about the flat band.

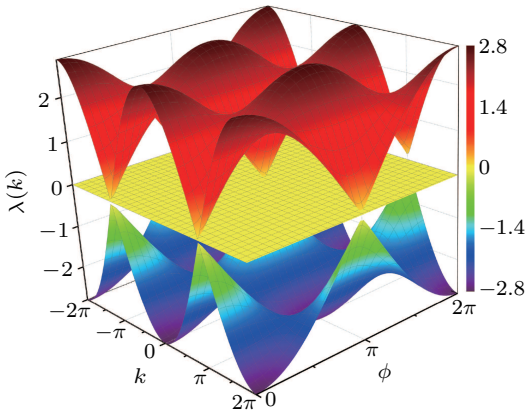


Fig. 2. Energy band $\lambda(k)$ *versus* wave number k for diverse magnetic flux ϕ. Note that the horizontal tilting $\varepsilon = 0$.

The wave functions for the eigenstates are

$$\begin{aligned}
&\{\psi_{\text{ga}}, \psi_{\text{gb}}, \psi_{\text{gc}}\} \\
&= \{[1+\cos(k+\phi)]/[1+\cos(k-\phi)], 0, -1\}, \qquad (8) \\
&\{\psi_a, \psi_b, \psi_c\}_{\pm} \\
&= \{1, \pm\sqrt{2}\sqrt{2+\cos(k-\phi)+\cos(k+\phi)}, 1\}, \qquad (9)
\end{aligned}$$

for the flat and dispersive bands respectively and are shown in Fig. 3, in Subsection 3.2.

3.2. Evolution

To characterize the evolution of the ground state, we define the total amplitude in a unit cell as $p_{\text{g}} = |\psi_{\text{ga}}|^2 + |\psi_{\text{gb}}|^2 + |\psi_{\text{gc}}|^2$.

It can be seen in Fig. 3(a) that the maximum p_{g}, for the positive branch of dispersive energy band, occurs around the center of Brillouin zone $k = 0$ while the minimum is around its boundary $k = \pm\pi$ with magnetic flux $\phi = 0$. This can also be inferred from Eq. (10). However, with the increase of ϕ, the positions of the extrema for p_{gs} vary in the Brillouin zone. For the case of $\phi = \pi$, the maximum occurs around the boundary $k = \pm\pi$ while the minimum lies around the center $k = 0$ of the

Brillouin zone. The results are further amplified by the corresponding evolution of $|a_g|^2$, $|b_g|^2$, and $|c_g|^2$ with nonzero ϕ in Fig. 3(a1), 3(b1), and 3(c1), respectively. Note that the results with $\phi = 2\pi$ are the same as those with $\phi = 0$. The properties of the negative dispersive band are similar to the positive one, as shown in Figs. 3(c), 3(c1), 3(c2), and 3(c3), respectively.

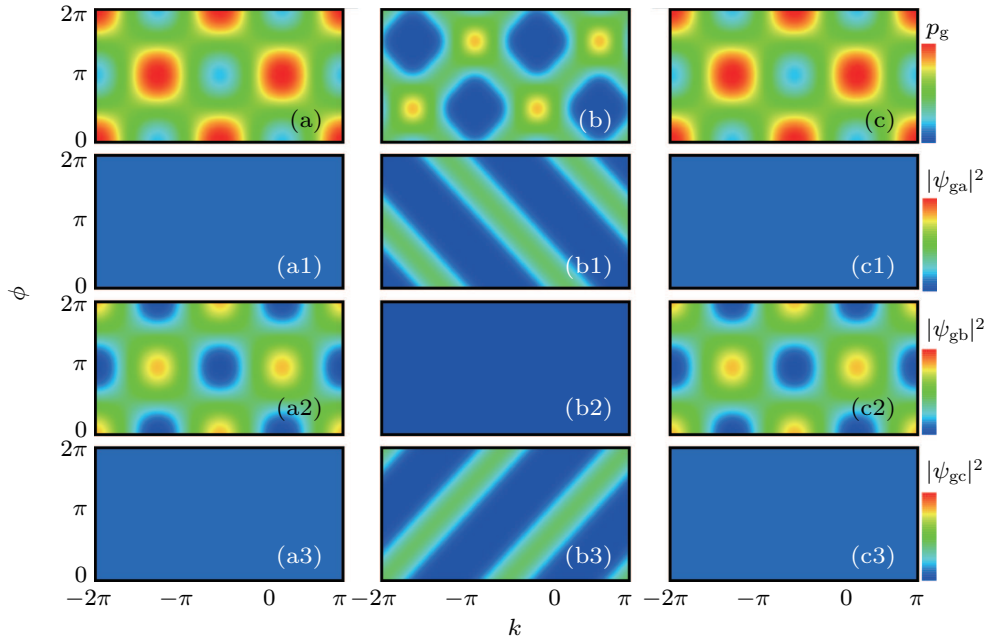


Fig. 3. The evolution of the ground wave functions in the plane composed of k–ϕ. Note that panels (a), (b), and (c) are for the total probability amplitudes p_g within each unit cell, which are by the superposition of probability amplitudes $|\psi_{ga}|^2$, $|\psi_{gb}|^2$, and $|\psi_{gc}|^2$ at a, b as well as c sites in diamond chain, respectively.

The scenario for the flat bands is entirely different as seen in Fig. 3(b), with the corresponding components as shown in Figs. 3(b1), 3(b2), and 3(b3). The positions of the extrema of p_g change with ϕ. For $\phi = \pi/2$, the maximum value exists around $k = \pi/2$ while the minimum value lies around $k = -\pi/2$, as shown in Fig. 3(b), 3(b1), 3(b2), and 3(b3).

4. Dynamical behaviors

In the last section, we considered the spectrum for $\varepsilon = 0$ and varying magnetic flux ϕ. Now, we consider the dynamical evolution of bosons with different initial configurations as shown in Fig. 4, motivated by the experimental realizations in optical lattices. Setting $\varepsilon = 0.05$, the dynamical evolution is described by the evolution of $p_n(t) = |a_n|^2 + |b_n|^2 + |c_n|^2$ for each unit cell (the gray region in Fig. 1). It should be noted that the wave packet center is at the 0th site at $t = 0$.

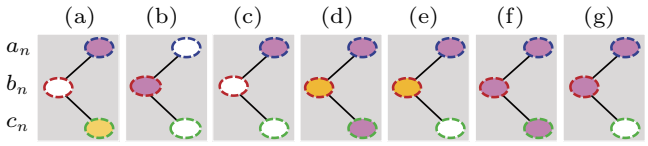


Fig. 4. Initial configurations of bosons in diamond chain. The circles filled with pink (yellow) represent the wave packet $e^{-n^2/2\sigma^2}$ ($-e^{-n^2/2\sigma^2}$) and the empty circles represent 0. For example, $\{a_n, b_n, c_n\} = (1, 0, -1)\, e^{-n^2/2\sigma^2}$ in panel (a). Note that $\sigma \equiv 10$.

4.1. The case in CLS

Figure 5 illustrates the effect of WMF on the tunneling dynamics for bosons with the initial distribution as its eigenstate $\{a_n, b_n, c_n\} = \frac{1}{\sqrt{2}}\{1, 0, -1\}\, e^{-n^2/2\sigma^2}$ (see Fig. 4(a)). Due to destructive interference and the local symmetries of the network, bosons are localized around certain sites in diamond chain.[26] The corresponding dynamical behaviors in individual chains are illustrated by $|a_n(t)|^2$ (uuper point in Fig. 4(a)), $|b_n(t)|^2$ (middle point in Fig. 4(a)), and $|c_n(t)|^2$ (lower point in Fig. 4(a)) of Ref. [5].

An external perturbation, such as an magnetic field, can open the energy gap and change the position of the extreme value for the wave function in the ground state for the system. A small ϕ ($\phi = 0.01$) can result in tiny band gaps and bosons localized around the 0th site can maintain its compact localized state for a while (from $t = 0$–400 in Fig. 5(b)). Due to destructive interference, bosons begin to oscillate along the direction of the lattice sites in the three chains (from $t = 400$–4000), which is demonstrated by $p_n(t)$ in Fig. 5(b), the corresponding $|a_n(t)|^2$ in Appendix A, see Fig. A3(a1), $|b_n(t)|^2$ in Fig. A3(a2), and $|c_n(t)|^2$ in Fig. A3(a3) of Appendix A, respectively. The existence of bosons in b chain (see Fig. A3(a2) implies the occurrence of the tunnelling among various chains, *i.e.*, Landau–Zener tunnelling. As time goes on, we find that,

the oscillations disappear gradually (from $t = 4000$–4400). Induced by WMF, collapses-revivals phenomena occur in diamond chain, which takes a long time and can be verified by the total time–space evolution of bosons as well as the single chain.

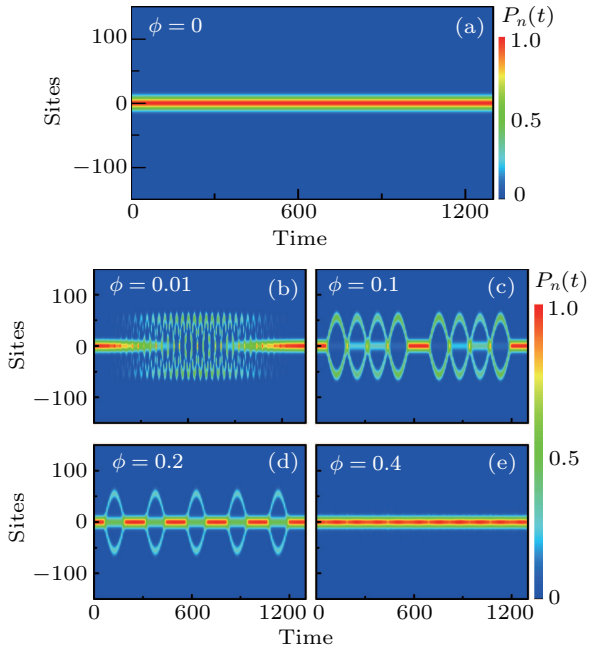


Fig. 5. The effect of WMF on the tunneling dynamics for bosons initially configured as Fig. 4(a).

When $\phi = 0.1$, Bloch oscillations with four period harvest absolutely from collapses-revivals phenomena, accompanying few localized bosons around the 0-th site in Fig. 5(c) (the evolutions in single chain are in Figs. A3(b1), A3(b2), and A3(b3)). Note that Landau–Zener tunnelling still happens among three chains. Figure 5(d) indicates that Bloch oscillations become entirely periodic when ϕ=0.2 and the exchange number of bosons among three chains is also nonzero, which is illustrated in Figs. A3(c1), A3(c2), and A3(c3), respectively. Providing $\phi = 0.4$, bosons are localized around the 0-th site again while Bloch oscillations vanish as the initial configuration is as shown in Fig. 5(e), which is further demonstrated by the single evolutions in Figs. A3(d1), A3(d2), and A3(d3), respectively. Note that bosons are still in the corresponding initial configuration, indicating zero exchange of bosons among the three chains.

Due to interference phenomenon, collapses-revivals phenomena harvest from localization phenomena partly by the means of Landau–Zener tunnelling when the initial configuration is in the eigenstate. In the presence of WMF, collapses-revivals phenomena, Landau–Zener tunneling, Bloch oscillations, and localization phenomena can always counteract and are complementary with each other in diamond chains.

4.2. The case not in CLS

Figure 6 illustrates the effect of WMF on the dynamical behavior of bosons, which are initially distributed as Fig. 4(b) (bosons only exist in b chain at $t = 0$). With $\phi = 0$, Bloch oscillations existed in the three chains from the -150th to the 150th site, whose analytical expression for the oscillation period T_0 is as Eq. (11) and figure A1 in Appendix A demonstrates the dependencies between T_0 and k. Note that the analytical T_0 almost matches with the numerical results, which can also be inferred from Fig. A2 in Appendix A.

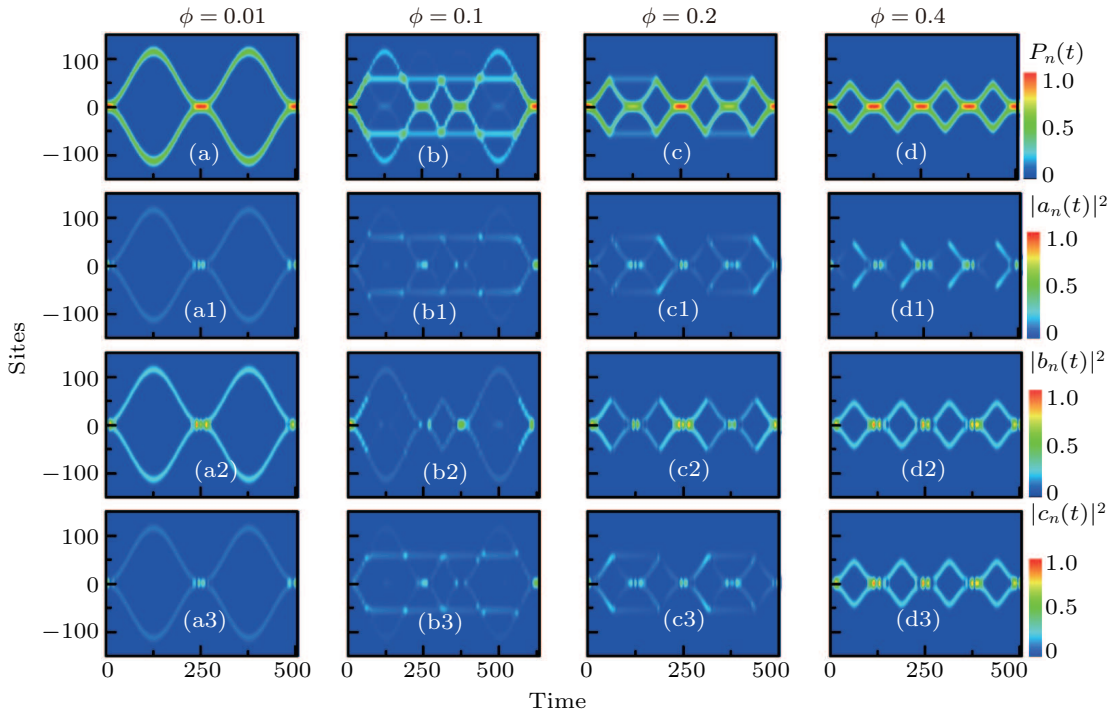


Fig. 6. The same as Fig. 5, but the initial configuration as Fig. 4(b) is not the eigenstate for the system.

With the increase of WMF, we find that, the mode for Bloch oscillations varies from only one frequency to multiple frequencies and the tunneling process becomes intricate. When $\phi = 0.1$, all bosons tunneling bidirectionally along the left and the right direction, which are named as the negative and the positive direction. Resulted from the symmetry of the oscillations in both directions, here we just consider the oscillations in the positive direction. Figure 6(b) shows that bosons existing in the 75-th site are separated to tripartite parts, some continue the original path until the 150-th site, some tunneling in the 75-th unit cell (tunneling happens among a, b, and c chains) and the rest bosons return to the 0-th site, induced by the energy gap opened by the WMF. Bosons will gather at the 75-th sites later, which will experience a similar process as before (divided to three parts) and they all arrive the 0-th site eventually. This dynamical process repeats as the progress in time, as shown in Figs. 6(b1), 6(b2), and (b3), respectively. With the further intensifying ϕ ($\phi = 0.2$), the tunneling dynamics is analogous to that in Fig. 6(a) with the range of sites for Bloch oscillations shrinking by a half except for the bosons staying at the 75-th site (see Figs. 6(c), 6(c1), 6(c2), and 6(c3), respectively), whose energy bands are in microgap. When $\phi = 0.4$, the tunneling dynamics is the same as that in Fig. 6(a) except for the halved range of site for Bloch oscillations in Figs. 6(d), 6(d1), 6(d2), and 6(d3), respectively.

When bosons are not distributed as the eigenstate initially, WMF may open tiny band gaps between the energy levels of the system, resulting in various dynamical behaviors of bosons in diamond chain, *i.e.*, collapses–revivals phenomena, Landau–Zener tunneling, Bloch oscillations, and localization phenomenon.

The similar dynamical phenomena can also be observed by the time–space evolution of bosons with configurations as shown in Figs. 4(c), 4(d), and 4(e) and in Figs. A4, A5, and A6. Note that the dynamical process of bosons with initial configurations as Figs. 4(f) and 4(g) are similar to those in Figs. 4(d) and 4(e), but in the opposite lattice direction.

5. Conclusion

Considering a diamond chain subjected to weak magnetic flux, the characteristics of the ground states and the energy band structure have been investigated for the system. We observed that transitions between different quantum phenomena depend on the weak magnetic flux and the initial configurations of bosons. This work can be extended to two dimensions with interactions, which will be intriguing and may reveal interesting physics.

Acknowledgment

One of the authors (Nana Chang) would like to thank "Center for Theoretical Physics of Complex Systems, Institute for Basic Science (IBS)" for hospitality, specially to its members: Dr. Pramod Padmanabhan, Dr. Arindam Mallick, Dr. Niladri Gomes, and Dr. Anton Parafilo for useful discussions.

Appendix A: Supporting materials

A1. The expression of tunneling period for oscillations

There holds the analytical expression of tunneling period for oscillations,

$$T(0) = \frac{2\pi}{\min\{\Delta\lambda\}} = \frac{\pi}{\sqrt{1+\cos k\cos\phi}}, \tag{A1}$$

where $\Delta\lambda$ represents the energy gap.

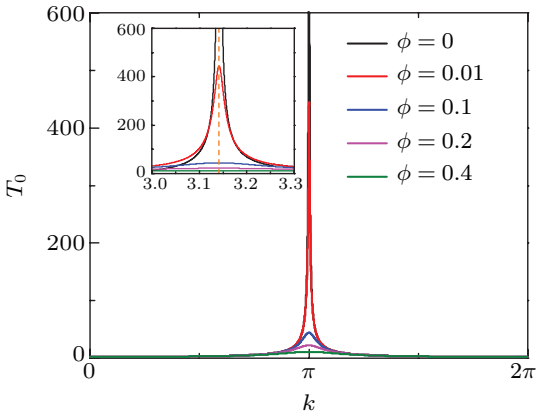


Fig. A1. The oscillation period T_0 for k with various ϕ. Note that the orange dotted line is $k = \pi$.

We find that the oscillation period T_0 closes to infinity at $k = \pi$ (see the orange dotted line illustrated in Fig. A1), which implies that bosons will not tunnelling among different lattices, *i.e.*, they are localized around the lattices initially configured (see Fig. 5(a)).

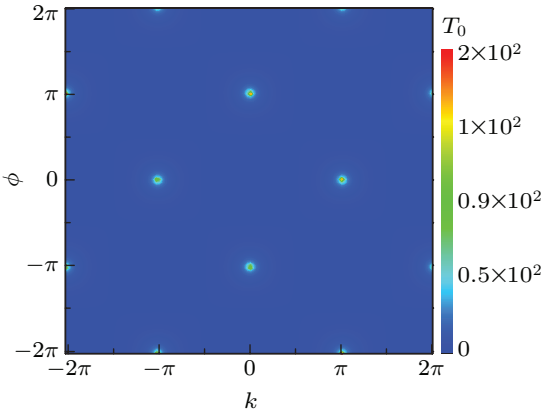


Fig. A2. The oscillation period T_0 in the plane of k–ϕ, which matches well with Fig. A1. Note that the orange dotted line is $k = \pi$.

A2. Dynamical behaviors

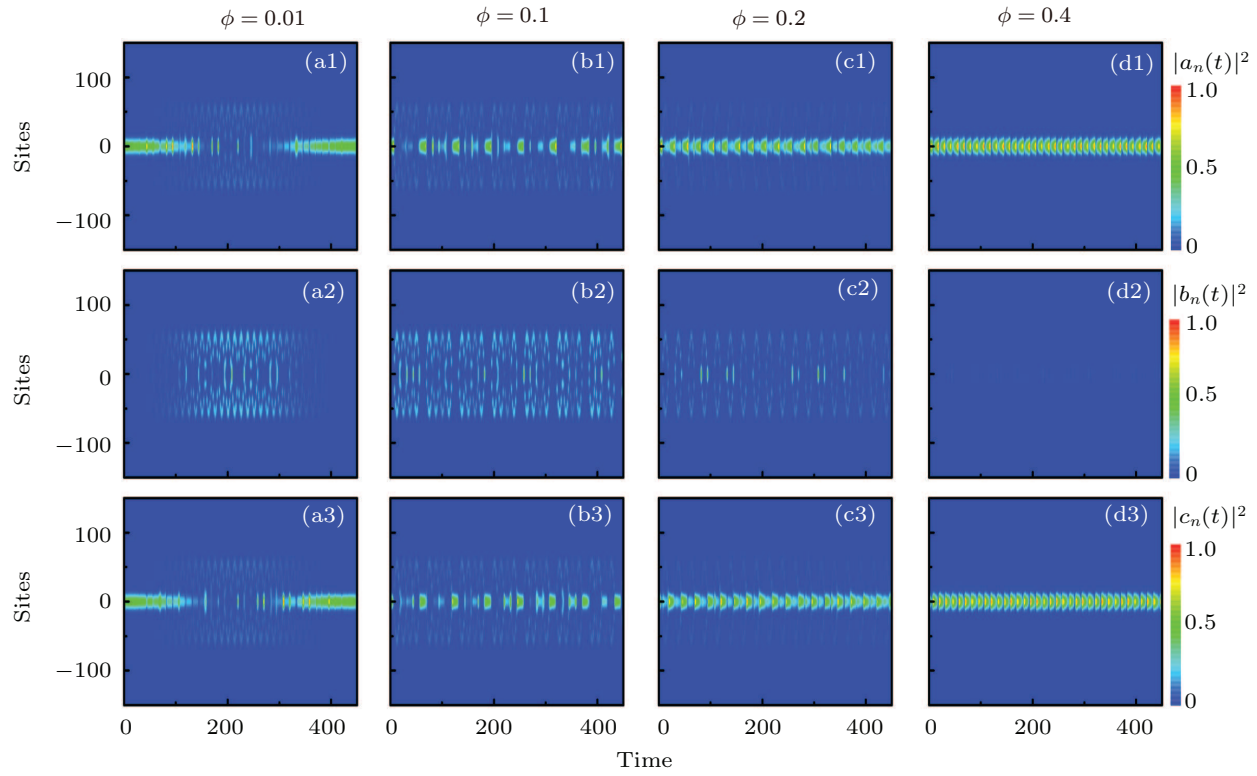


Fig. A3. The dynamical evolution of bosons with initially configuration as shown in Fig. 4(a).

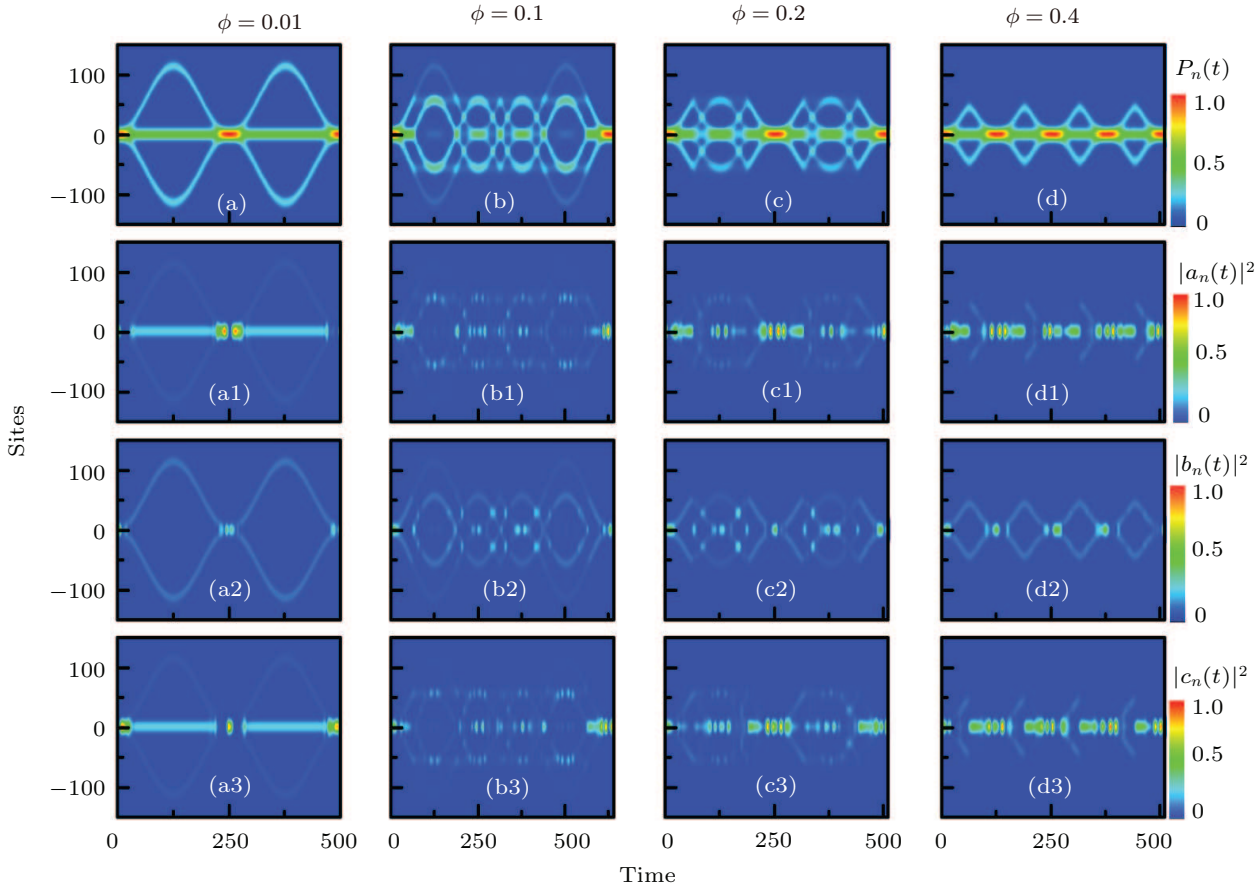


Fig. A4. The same as Fig. 6, but for the initial configuration as shown in Fig. 4(c).

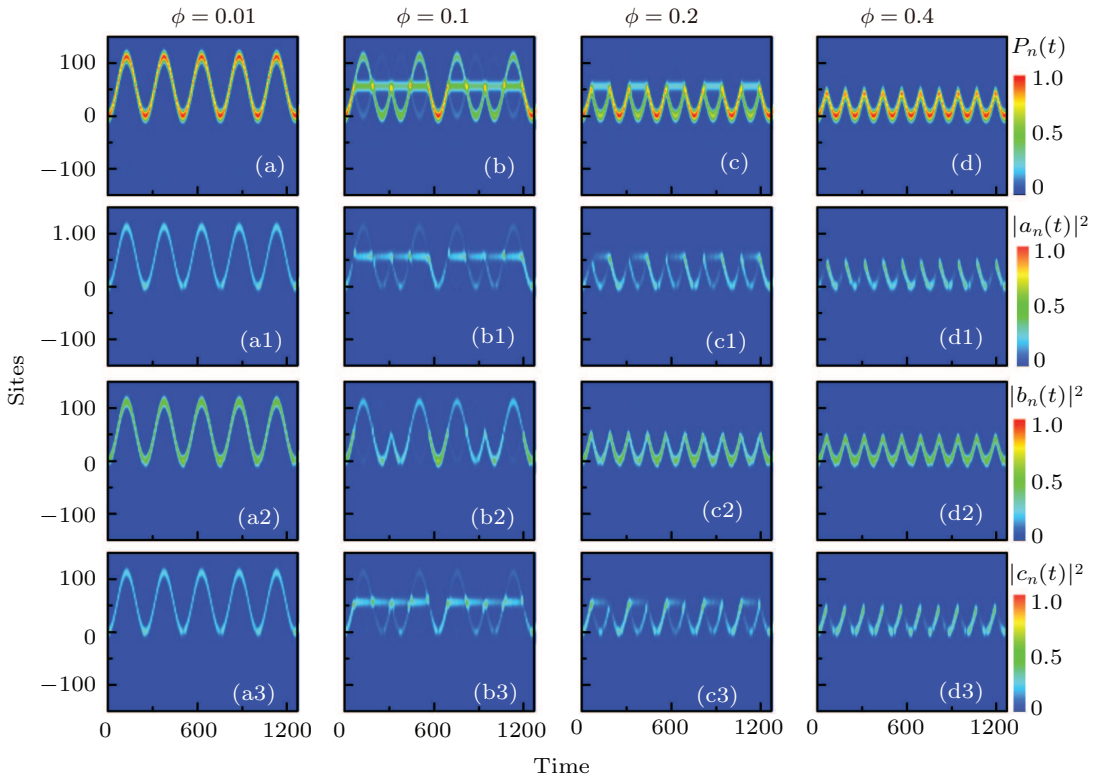


Fig. A5. The same as Fig. 6, but for the initial configuration as shown in Fig. 4(d).

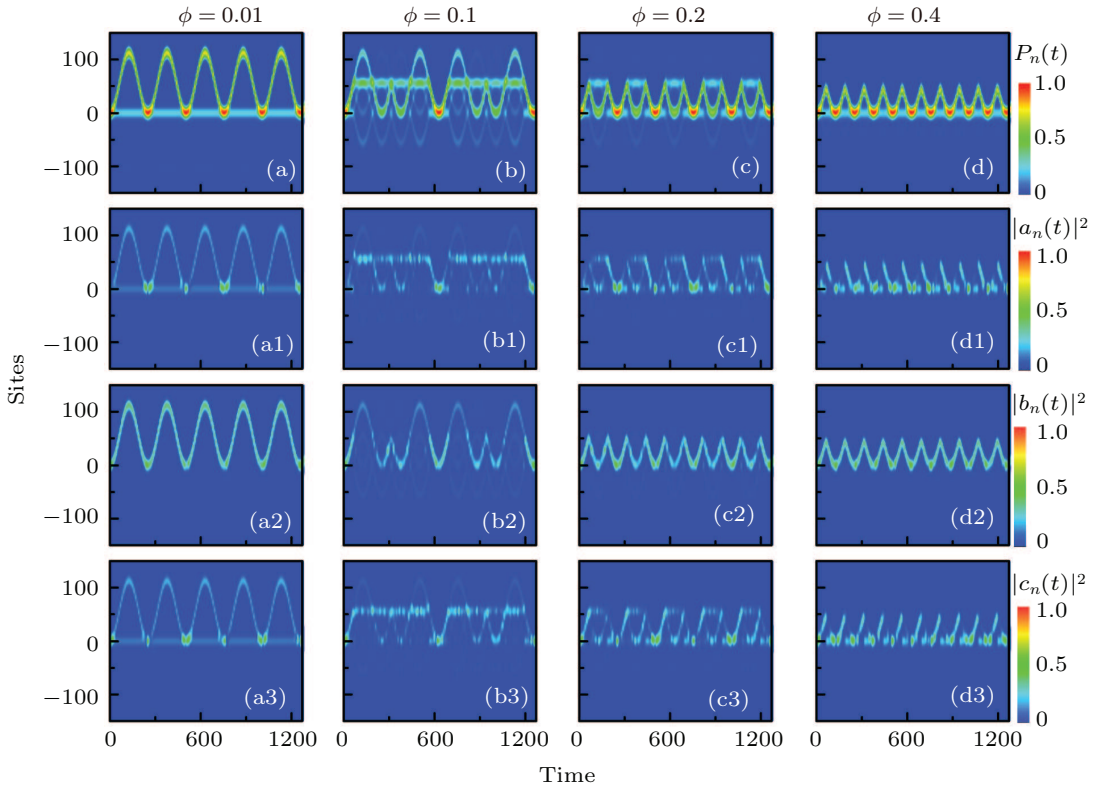


Fig. A6. The same as Fig. 6, but for the initial configuration as shown in Fig. 4(e).

References

[1] Anderson M H, Matthews M R, Wieman C E and Cornell E A 1995 *Science* **269** 198

[2] Schmitt J, Damn T, Dung D, Vewinger F, Klaers J and Weitz M 2014 *Phys. Rev. Lett.* **112** 030401

[3] Trombettoni A and Smerzi A 2001 *Phys. Rev. Lett.* **86** 2353

[4] Cazalilla M A, Citro R, Giamarchi T, Orignac E and Rigol M 2011 *Rev. Mod. Phys.* **83** 1405

[5] Chang N N and Xue J K 2018 *Chin. Phys. B* **27** 105203

[6] Khomeriki R and Flach S 2016 *Phys. Rev. Lett.* **116** 245301
[7] Guláacsi Z, Kampf A and Vollhardt D 2007 *Phys. Rev. Lett.* **99** 026404
[8] Mikeska H J and Luckmann C 2008 *Phys. Rev. B* **77** 054405
[9] Kobayashi K, Okumura M, Yamada S, Machida M and Aoki H 2016 *Phys. Rev. B* **94** 214501
[10] Dalibard J, Gerbier F, Juzeliunas G, *et al.* 2011 *Rev. Mod. Phys.* **83** 1523
[11] Gerbier F and Dalibard J 2010 *New J. Phys.* **12** 033007
[12] Zhang X, Yu Z F and Xue J K 2016 *Chin. Phys. Lett.* **33** 40302
[13] Zhou W Y, Wu Y J and Kou S P 2018 *Chin. Phys. B* **27** 050302
[14] Dodaro J F, Kivelson S A, Schattner Y, *et al.* 2018 *Phys. Rev. B* **98** 075154
[15] Wang Y F, Gu Z C, Gong C D and Sheng D N 2011 *Phys. Rev. Lett.* **107** 146803
[16] Wen J, Kargarian M, Vaezi A, *et al.* 2011 *Phys. Rev. B* **84** 235149
[17] Du L, Chen Q, Barr A D, *et al.* 2018 *Phys. Rev. B* **98** 245145
[18] Creffield C E, Pieplow G, Sols F, *et al.* 2016 *New J. Phys.* **18** 093013
[19] Aidelsburger M, Atala M, Lohse M, Barreiro J T, Paredes B and Bloch I 2013 *Phys. Rev. Lett.* **111** 185301
[20] Cartwright C, Chiara G D and Rizzi M 2018 *Phys. Rev. B* **98** 184508
[21] Bouwmeester D, Dekker N H, Dorsselaer F E V, Schrama C A, Visser P M and Woerdman J P 1995 *Phys. Rev. A* **51** 646
[22] Yan J Y, Duan S Q, Zhang W and Zhao X G 2009 *Phys. Rev. A* **79** 053613
[23] Niu Q and Raizen M G 1998 *Phys. Rev. Lett.* **80** 3491
[24] Loladze V and Khomeriki R 2017 *Phys. Rev. E* **95** 042204
[25] Longhi S and Valle G D 2012 *Phys. Rev. A* **86** 043633
[26] Flach S, Leykam D, Bodyfelt J D, Matthies P and Desyatnikov A S 2014 *Europhys. Lett.* **105** 30001
[27] Huber S D and Altman E 2010 *Phys. Rev. B* **82** 184502
[28] Aoki H, Ando M and Matsumura H 1996 *Phys. Rev. B* **54** 17296
[29] Bilitewski T and Moessner R 2018 *Phys. Rev. B* **98** 235109
[30] Chang N N, Yu Z F, Zhang A X and Xue J K 2017 *Chin. Phys. B* **26** 115202
[31] Vicencio R A, Cantillano C, Inostroza L M, Real B, Cortés C M, Weimann S, Szameit A and Molina M I 2015 *Phys. Rev. Lett.* **114** 245503
[32] Real B and Vicencio R A 2018 *Phys. Rev. A* **98** 053845
[33] Kimura T, Tamura H, Shiraishi V and Takayanagi H 2002 *Phys. Rev. B* **65** 081307
[34] Gligorić G, Maluckov A, Hadžievski Lj, Flach S and Malomed B A 2016 *Phys. Rev. B* **94** 144302
[35] Johansson M, Naether U and Vicencio R A 2015 *Phys. Rev. E* **92** 032912